



Article

Electron Beam Brightness and Undulator Radiation Brilliance for a Laser Plasma Acceleration Based Free Electron Laser

Amin Ghaith ^{1,*}, Alexandre Loulergue ¹, Driss Oumbarek ¹, Olivier Marcouillé ¹, Mathieu Valléau ¹, Marie Labat ¹, Sebastien Corde ² and Marie-Emmanuelle Couprie ¹

¹ Synchrotron Source Optimisée de Lumière d'Énergie Intermédiaire du LURE (Laboratoire pour l'Utilisation du Rayonnement Electromagnétique) (Synchrotron SOLEIL), L'Orme des Merisiers, 91190 Saint-Aubin, France; alexandre.loulergue@synchrotron-soleil.fr (A.L.); driss.oumbarek-espinos@synchrotron-soleil.fr (D.O.); olivier.marcouille@synchrotron-soleil.fr (O.M.); mathieu.valleau@synchrotron-soleil.fr (M.V.); marie.labat@synchrotron-soleil.fr (M.L.); marie-emmanuelle.couprie@synchrotron-soleil.fr (M.-E.C.)

² École Nationale Supérieure de Techniques Avancées Paris (ENSTA Paris), Centre National de la Recherche Scientifique (CNRS), Ecole Polytechnique, Institut Polytechnique de Paris, 91128 Palaiseau, France; sebastien.corde@polytechnique.edu

* Correspondence: amin.ghaith@synchrotron-soleil.fr

Received: 3 December 2019; Accepted: 27 December 2019; Published: 1 January 2020



Abstract: We report here on spontaneous undulator radiation and free electron laser calculations after a 10-m long transport line (COXINEL) using a Laser Plasma acceleration (LPA) source. The line enables the manipulation of the properties of the produced electron beams (energy spread, divergence, dispersion) in view of light source applications. The electron beam brightness and undulator radiation brilliance are addressed by an analytical approach enabling us to point out the influence of chromatic effects in the COXINEL case.

Keywords: laser plasma acceleration; electron beam brightness; undulator radiation; free electron laser

1. Introduction

Particle accelerators have become a crucial need for advancement in many domains such as nanotechnology, atomic physics, nuclear physics, chemistry and medicine. By accelerating particles close to the speed of light, all kinds of explorations can be done, whether it is for colliding particles to discover elementary particles or by producing an intense x-ray source from synchrotron radiation, capable of unraveling the quantum realm.

A relativistic electron traversing a periodic sinusoidal magnetic field, generated by an undulator, emits synchrotron radiation at each period [1]. Photons produced by an individual electron interfere constructively resulting in sharp spectral lines well collimated within a cone. In a Free Electron Laser (FEL), the electrons interact with the radiation, where energy is transferred between the electron beam and the radiated wave via the so-called ponderomotive force. This process results in a low gain of the electromagnetic wave, firstly introduced using a quantum approach [2] and further examined using a classical approach [3]. In the undulator magnetic field, the beam energy modulation becomes a density modulation, because electrons with smaller energies are affected more by the field, prolonging their orbit and thus leading to a micro-bunching mechanism. Thanks to this process, the electrons are put in phase along the longitudinal axis and emit coherent radiation and light intensity is amplified. Unlike conventional lasers, where the electrons are bound to the atoms in the gain medium allowing the emission at a fixed wavelength, the FEL wavelength can be varied by changing the machine parameters

such as electron beam energy or/and undulator magnetic field. The FEL has thus become a conceptual and practical alternative and has exceeded by far other lasing systems. This new laser revolution, with the advent of X-Ray FEL, opens the path for deciphering unexplored ultra-fast phenomena with unprecedented time resolution.

Conventional linear accelerators (Linacs) are often used for FEL based applications, due to their stability and efficiency and, most importantly, to the large experience gained using these accelerators over many years. However, these infrastructures are large in size, especially for operating at higher energies and are limited to tens to hundreds of MeV/m accelerating gradient by the use of RF cavities. Following the rapid progress in the development of high-intensity laser systems [4], a new accelerating concept called Laser Plasma Acceleration (LPA) was introduced [5]. In an LPA, an intense short-pulsed laser is focused into a gas medium. Due to the high electric fields, electrons are stripped and separated spatially from the heavy ions that have a negligible response in the time-scale of that of the electrons. This process creates a plasma with a disequilibrium charge distribution in the perturbed region that can be observed as a wakefield (plasma wave) following the laser. A huge gradient of \sim GeV/m is created between the back of the wakefield (consisting mainly of electrons) and at its center (consisting mainly of ions), in which electrons trapped between these two regions are subjected to an extreme electric force. This allows LPA to operate with thousands of times gradients than ones in conventional accelerators, thus producing extremely compact sources of bright and energetic electrons [6–8].

Undulator radiation has already been measured using such a source [9–12] but not with the quality achieved on synchrotron radiation facilities. LPA based FEL [13] demonstration is still challenged by the electron beam quality. In this paper, the main setbacks posed by an LPA based electron beam, in the view of an FEL amplification, are reported, alongside solutions that can qualify such beams for an FEL application. Undulator radiation achieved so far with LPA beams is discussed, including the COXINEL experiment equipped with an advanced manipulation line. The paper presents combined analytic approaches for electron beam manipulation in the LPA transfer line starting from the source parameters to the ones at the undulator center, undulator radiation and FEL calculations. Emphasis is put on the electron beam brightness evolution and undulator brilliance. Finally, the FEL performance is examined for different initial electron beam parameters for the COXINEL baseline reference case.

2. Issues of LPA Based FEL

The FEL amplification efficiency highly depends on the overlapping of the electron beam and the FEL wave. Thus, there should be a proper transverse matching (size, divergence) between the electron beam and the FEL wave along the undulator for ensuring a proper interaction. Besides, the normalized emittance ϵ_n should satisfy the Pellegrini criterion [14]:

$$\epsilon_n < \frac{\gamma \lambda_{FEL}}{4\pi} \quad (1)$$

where γ is the relativistic factor and λ_{FEL} the operating FEL wavelength. For a typical LPA electron beam of 500 MeV and $\epsilon_n = 1$ mm·mrad at the source, the emittance requirement is satisfied for an operating wavelength $\lambda \geq 12$ nm. However, unlike beam drifts in conventional accelerators where the ϵ_n scales as $\gamma \epsilon_{eff}$ (ϵ_{eff} being the effective emittance), a problem arises regarding the transport, where the chromatic emittance ϵ_{chrom} increases quadratically with the divergence along a distance s [15–18]. Such dependence can be understood by using the general definition of the normalized emittance expressed as [19]:

$$\epsilon_n^2 = \langle x^2 \rangle \langle \gamma^2 x'^2 \rangle - \langle x \gamma x' \rangle^2, \quad (2)$$

where x and x' are the position and angle of the particle with respect to the reference path, respectively and $\langle \rangle$ stands for the average. Considering that there is no correlation between the energy and the transverse position, that is drift without collective effects, one finds:

$$\varepsilon_n^2 = \langle \gamma^2 \rangle \langle x^2 \rangle \langle x'^2 \rangle - \langle \gamma \rangle^2 \langle x x' \rangle^2, \quad (3)$$

Inserting the energy spread σ_γ relation:

$$\sigma_\gamma^2 = \frac{\langle \gamma^2 \rangle - \langle \gamma \rangle^2}{\langle \gamma \rangle^2}$$

in Equation (3), one gets:

$$\varepsilon_n^2 = (\sigma_\gamma^2 \sigma_x^2 \sigma_x'^2 + \varepsilon_{eff}^2) \langle \gamma \rangle^2, \quad (4)$$

where σ_x and σ_x' are the beam size and divergence, respectively. If the chromatic emittance is negligible, the first term in Equation (4) is set to zero and one arrives to the conventional definition of the normalized emittance as $\varepsilon_n = \langle \gamma \rangle \varepsilon_{eff}$. In the case of LPA, the generated electron beam can be considered as a point source, thus the bunch transverse size after a drift distance s becomes:

$$\sigma_x(s) = \sigma_x' s \quad (5)$$

Inserting Equation (5) in Equation (4), one gets the expression of the emittance after a drift s in the longitudinal direction:

$$\varepsilon_n^2(s) \approx \varepsilon_{n0}^2 + \gamma \sigma_\gamma^2 \sigma_{x,z}^4 s^2. \quad (6)$$

For a typical LPA electron beam of 2 mrad divergence, 500 MeV energy and 1% spread, the emittance is increased by a factor of 80 just after 10 cm drift, thus the divergence should be handled at an early stage of the transport.

The second FEL requirement concerns the electron beam energy spread. A large energy spread deteriorates the micro-bunching efficiency and smears out the electron bunch [20]. Hence, the electron beam should be rather cold with relative energy spread σ_γ smaller than the FEL bandwidth that is equal to the Pierce parameter ρ_{FEL} :

$$\sigma_\gamma < \rho_{FEL}, \quad (7)$$

where

$$\rho_{FEL} = \left[\frac{I}{8\gamma^3 I_A} \left(\frac{\lambda_u K_u |JJ|}{2\pi\sigma_x} \right)^2 \right]^{1/3},$$

where I is the electron beam current, $I_A = 17$ kA the Alfvén current, λ_u the undulator period, $K_u = 93.4B[T]\lambda_u[m]$ the deflection parameter, B the magnetic field, $|JJ| = \left| J_1(Y) - J_0(Y) \right|^2$, J the Bessel function and $Y = \frac{K_u^2}{4(1+K_u^2/2)}$. ρ_{FEL} is the decisive parameter in terms of FEL amplification, such that the gain length L_g , saturation length L_{sat} and saturation power P_{sat} are dependent on it as follows:

$$L_g = \frac{\lambda_u}{4\pi\sqrt{3}\rho_{FEL}}, \quad L_{sat} \approx 20L_g, \quad P_{sat} \approx \rho_{FEL}IE, \quad (8)$$

where E is the electron energy. ρ_{FEL} is normally of the orders of 10^{-3} , so an energy spread of 0.1% and below is required to enable the FEL amplification. This condition is not accomplished by typical LPA, since energy spreads have been measured to be $\sim 10^{-2}$ for MeV-GeV electron beams [21,22].

Furthermore, the bunch length is ultrashort of the orders of a few μm . This reduces the interaction length of the radiation field with the electron bunch.

2.1. Electron Beam Divergence Handling

Focusing magnets are used to handle and transport electron beams inside an accelerator. The focusing strength K is proportional to G/P , where G is the magnetic field gradient, P the beam

momentum so that a large gradient is needed for high energies. In the case of an LPA beam, a typical gradient of >100 T/m is required. The conventional focusing magnets are electro-magnet based quadrupoles providing an intermediate gradient and wide tunability. However, the device has to be compact in order to achieve a high gradient which poses a mechanical complexity. Superconducting magnets come in handy for such applications but they are much more expensive than the conventional electro-magnets due to the cryogenic cost (installation and operation) and the possibility of a quench as a result of heating originating from synchrotron radiation and image charges. Permanent magnet based quadrupoles eliminate the need for power supplies, cables and the large element of infrastructure for the water cooling system and can be reduced in size without losing the magnetic field strength making them suitable for compact applications such as LPA [23].

In view of an LPA application, an alternative focusing system, a plasma lens generating a field gradient of $\sim kT/m$, can be used to focus the electron beam at an early stage by the use of the plasma itself. The plasma lens is based on the concept of a magnetically self-focusing electron beam of density n_e by ions from a residual gas or more generally by a plasma of density n_p [24]. Two regimes can be implemented, an over-dense regime ($n_e \ll n_p$) producing a focusing strength of $K = 2\pi r_e n_e / \gamma$ with r_e the classical radius of the electron [25] and under-dense regime ($n_e \gg n_p$) with a strength of $K = 2\pi r_e n_p / \gamma$. Afterward, a passive plasma lens has been proposed and developed [26,27] and tested for an LPA experiment [28]. Another type, active plasma lens, has been proposed [29,30] and applied to ion beams [29,31] and to LPA applications as well [32–36].

2.2. Energy Spread Handling

Solutions to handle the FEL second requirement are now examined.

A magnetic chicane can be introduced in the line to stretch the electron beam and reduce the slice energy spread while inducing an energy-position correlation. A combined scaling law of the energy spread and bunch length [37,38] showed that the FEL gain length, in the case of bunches with relative energy spread on the order of the Pierce parameter and bunch lengths on the order of the cooperation length can be reduced. Furthermore, a set of quadrupoles can be placed between the chicane and the undulator, taking advantage of the correlation and allowing for chromatic optics [39]. Using this optics, the different energy slices are focused at different locations inside the undulator. With the right synchronization between the chromatic focusing and the wave slippage, one is able to ensure that the FEL wave always sees the maximum electron density and thus improving the FEL gain.

Another solution is the implementation of a Transverse Gradient Undulator (TGU) that can be used in the FEL based LPA line to compensate for the effects of beam energy spread. By canting the poles and magnets, one can generate a linear dependence of the vertical undulator field. The electron beam is dispersed in the horizontal axis so that each energy slice undergoes a different field magnitude and emit radiation at the same wavelength. This process enhances the FEL performance as shown in References [40,41].

3. LPA Based Undulator Radiation

The feasibility of achieving undulator radiation with an LPA source has been demonstrated in different laboratories.

3.1. Institute fur Optik und Quantenelektronik

A high-intensity Titanium:Sapphire laser of 5×10^{18} W·cm⁻² and pulse duration of 80 fs is used to produce the relativistic electron beams [9]. The laser pulse is focused by an off-axis parabolic mirror into a supersonic helium gas jet where it accelerates electrons to several tens of MeV energy. The electrons propagate through an undulator, producing synchrotron radiation and into a magnetic electron spectrometer. Radiation is collected by a lens and analyzed in an optical spectrometer. The electron spectrum peaked at 64 MeV has a width of 3.4 MeV (full-width at half-maximum, FWHM), that is, rms energy spread of $\sim 2.3\%$ and contains a charge of 28 pC. The normalized emittance of the beam is

estimated to be $\varepsilon_n \approx 1.3 \pi \text{ mm}\cdot\text{mrad}$, derived from beam optics simulations and the beam divergence measured from the beam size. The undulator radiation is measured using a spectrometer. The spectra are peaked at 740 nm with a bandwidth of 55 nm and contain 284,000 photons (black). Another peak is observed at a wavelength of 900 nm (red) produced by a 58 MeV, 14 pC and 5% energy spread in another shot.

3.2. Max-Planck-Institut für Quantenoptik

The line is customized to generate soft-X-ray undulator radiation with LPA electron beams [10]. Quadrupoles of bore radius 3 mm with an adjustable longitudinal position, achieving a gradient of 500 T/m, are installed after the electron source. The laser pulse is focused on a gas cell, where the electron beam is generated and then focused by two quadrupoles into the undulator. Diagnostic equipment, composed of an electron and photon spectrometer, are placed at the end of the line. An electron beam centered around the energy 210 MeV is measured using an electron spectrometer resulting in undulator radiation peaked at 18 nm (first harmonic) and 9 nm (second harmonic) using a monochromator with first diffraction order and a CCD camera.

3.3. Laboratoire d'Optique Appliquée

At Laboratoire d'Optique Appliquée, the line is designed for the generation of UV undulator radiation with laser-plasma-accelerated electron beams [11]. A Titanium:Sapphire laser delivering a linearly polarized pulse at 800 nm with more than 1 J energy, about 30 fs duration is focused on a gas jet made of Helium leading to an electron density of $5 \times 10^{18} \text{ cm}^{-3}$. The generated relativistic electrons pass through a triplet of permanent magnet quadrupoles placed 15 cm from the source providing 15.4 T/m, -25 T/m and 15 T/m gradients, followed by a 0.6 m long undulator of period 18.2 mm and a deflection parameter of 1. The photon beam transverse shape radiation is measured on the CCD camera, which images a position corresponding to 60 cm after the end of the undulator and for electron energy of 120 MeV energy.

3.4. SUPA, Department of Physics, University of Strathclyde

An Advanced Laser-Plasma High-energy Accelerators towards X-rays (ALPHA-X) accelerator beam line has been commissioned [12]. A Titanium:Sapphire laser pulse centered at a wavelength of 800 nm with full-width at half-maximum duration of 36 fs and peak intensity of $2 \times 10^{18} \text{ W}\cdot\text{cm}^{-2}$ is focused to a 20 μm waist at the leading edge of a 2 mm diameter Helium gas jet to form a relativistic self-guided plasma channel. The electron beams produced are initially collimated using a triplet of miniature permanent magnet quadrupoles of fixed gradients of 500 T/m. A triplet of electromagnetic quadrupoles then focuses the beam through the undulator with gradient $\sim 2.4 \text{ T/m}$. Undulator output radiation is detected using a vacuum scanning monochromator and a CCD camera. The energy distribution measured has mean central energy of 104 MeV, with a 5% relative energy spread and contains a mean charge of $1.1 \pm 0.8 \text{ pC}$. The mean spectral bandwidth of the radiation is $69 \pm 11 \text{ nm}$ corresponding to a relative bandwidth of $32 \pm 7\%$, decreasing to as low as 16%.

Table 1 summarizes some of the undulator radiation characteristics observed so far using an LPA source. The measured radiation bandwidth is still quite wide with rather poor wavelength stability. Wavelength tunability with undulator gap adjustment has not been shown yet. The undulator radiation quality achieved so far does not yet reach what is currently achieved on storage ring accelerator-based light sources.

Table 1. Laser and undulator characteristics used for the experiment, alongside the radiation quality produced. I the laser intensity, λ_L the laser wavelength, E energy of the produced electron, λ_u the undulator period, N_u undulator number of periods, K_u the deflection parameter, λ the undulator radiation wavelength, $\Delta\lambda/\lambda$ the relative bandwidth, \mathfrak{B} the radiation brilliance.

Parameter Unit	LPA System			Undulator			Radiation		
	I $\text{W}\cdot\text{cm}^{-2}$	λ_L nm	E MeV	λ_u mm	N_u	K_u	λ nm	$\Delta\lambda/\lambda$ %	\mathfrak{B} $\text{ph/s/mm}^2/\text{mrad}^2/0.1\%\text{bw}$
[9]	5×10^{18}	740	65	20	50	0.6	740	7.4	6.5×10^{16}
[10]	-	-	210	5	60	0.55	18	30	1.3×10^{17}
[11]	-	800	120	18	30	1	230-440	18	-
[12]	2×10^{18}	800	105	-	100	0.38	160-220	16	1×10^{18}

3.5. COXINEL Experiment

The COXINEL transport line [42,44], as shown in Figure 1, starts with the LPA system driven by a Titanium:Sapphire laser at Laboratoire d'Optique Appliquée, which delivers 30 fs (FWHM) pulses of 1.5 J energy at a central wavelength of 800 nm with a repetition rate of 1 Hz, power of 30 TW and energy of 1.5 J. The laser beam is focused by an off-axis parabola into a gas mixture composed of 99% He and 1% N₂.

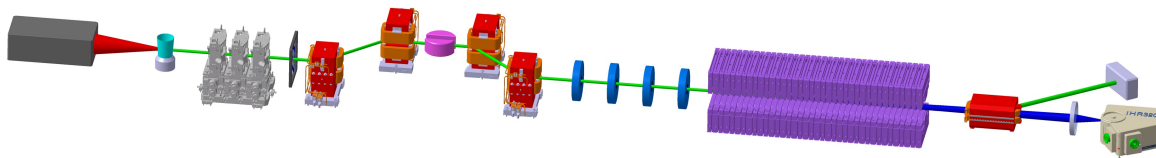


Figure 1. COXINEL beam line starting with the laser hutch (dark grey), gas jet (blue), a triplet of quadrupoles (grey), four dipoles (red), another set of quadrupoles (blue), undulator (purple) and a dipole dump (red).

The first magnetic element is a triplet of tunable high gradient permanent magnet-based quadrupoles (QUAPEVA) [23,45,46], placed 5 cm from the electron source. The triplet strongly focuses the LPA electron beam and permits to handle the large divergence at an early stage of the transport and mitigate the emittance growth. The electron beam is then sent through a chicane, where the beam is longitudinally stretched and sorted in energy to reduce the slice energy spread. The presence of a variable width slit in the middle of the chicane enables to select an energy range of interest [47–49]. A second set of quadrupoles placed after the chicane ensures that the transverse beam size is minimized at the undulator center. The undulator is a cryo-ready one operating at room temperature [50–52]. Table 2 presents the magnetic elements characteristics of the line. The QUAPEVAs achieve a maximum gradient of ~ 180 T/m and provide tunability of ~ 90 T/m. The chicane is composed of four electro-magnet dipoles. The electro-magnet based quadrupoles generate a maximum gradient of 20 T/m. The undulator is 2 m long and of period 18.16 mm with an adjustable magnetic gap providing a field variation. Transfer line components and LPA laser are aligned within ± 100 μm on the reference axis using a laser tracker.

Table 2. COXINEL magnets relevant parameters. The three values for PMQs are for each PMQ of the triplet in the beam propagation order.

	Unit	Value
Permanent magnet quadrupoles		
Magnetic length	mm	40.7; 44.7; 26
Minimum gradient	T/m	98; −100; 90
Maximum gradient	T/m	181; −184; 165
Bore radius	mm	4
Chicane dipoles		
Magnetic length	mm	208.33
Integrated field	T·mm	130
Maximum R_{56}	mm	32
Maximum field	T	0.53
Electro magnet quadrupoles		
Magnetic length	mm	213.3
Maximum gradient	T/m	20
Bore radius	mm	12
Steerers		
Maximum integrated field	G.m	38
Undulator		
Period	mm	18.16
Number of periods	-	107
Minimum gap	mm	4.5
Maximum field	T	1.2

The electron beam has been successively controlled and transported down to the undulator. Thanks to the QUAPEVAs, beam pointing alignment compensation was established that enabled to correct the electron beam dispersion and transport it to the undulator [43]. An electron monochromator is added in the middle of the chicane enabling to select a smaller range of energies. This enables us to map the photon transverse shape using a CCD camera [43]. In addition, new electron beam optics has been adopted afterward, that enabled to reduce the energy spread of the electron beam arriving at the undulator more efficiently. This enabled us to reach a minimum undulator radiation bandwidth of 2% [53].

3.6. LUX at CFEL

Undulator radiation has also been reported [54] using a Titanium:Sapphire laser of 200 TW power to generate electrons at energies 600 MeV. The undulator is of a period of 5 mm and a K_u value of 0.3, generating radiation at a wavelength of nm.

4. Electron Beam Characteristics in the COXINEL Line

4.1. Transport

The COXINEL line was designed to enable wide tuning and manipulation of the electron beam. Thanks to the tunable high gradient QUAPEVAs, different beam optics can be adopted. Electron beam transport is tuned with BETA code [55] up to the second order, with home-made multiparticle tracking code for high order non-linear effects and collective effects like coherent synchrotron radiation [56]. Hard-edge models are used for the magnets and apertures of the vacuum chamber along the beam line are included. A linear optics from source to image [39] is implemented. This optics ensures a minimum beam size (waist) for the on-momentum particles (energy deviation $\delta = 0$) at the focusing point (undulator center). By neglecting the coupling effect and limiting to the horizontal plane and chromatic terms, the transfer matrix from source to image can be expanded up to the second order as [57]:

$$\begin{pmatrix} x \\ x' \end{pmatrix} = \left[\begin{pmatrix} R_{11} & R_{12} \\ R_{21} & R_{22} \end{pmatrix} + \delta \begin{pmatrix} R_{116} & R_{126} \\ R_{216} & R_{226} \end{pmatrix} \right] \begin{pmatrix} x_0 \\ x'_0 \end{pmatrix}, \quad (9)$$

where the matrix R_{ij6} stands for the chromatic second order perturbation. The COXINEL line ensures minimum a chromatic effect induced by the energy spread such that the term R_{226} is very small. Also, the electron beam generated by an LPA starts as a point source, so some of the terms can be neglected. And by considering a round Gaussian beam and approximating that $R_{22} = 1/R_{11}$ [58], the rms associated momenta transfers at the center of the undulator can be expressed as:

$$\begin{cases} \sigma_x^2 = R_{11}^2 \sigma_{x0}^2 + R_{126}^2 \sigma_{x0}'^2 \sigma_\gamma^2 \\ \sigma_x'^2 = \frac{1}{R_{11}^2} \sigma_{x0}'^2 \\ \sigma_{xx'} = R_{126} \sigma_{x0}'^2 \sigma_\gamma / R_{11} \end{cases}, \quad (10)$$

Assuming a linear chicane decompression, the bunch length σ_l and slice energy spread $\sigma_{\gamma-slice}$ are expressed as:

$$\begin{cases} \sigma_l = \sqrt{\sigma_{l0}^2 + R_{56}^2 \sigma_\gamma^2} \\ \sigma_{\gamma-slice} = \frac{\sigma_{l0}}{\sqrt{\sigma_{l0}^2 + R_{56}^2 \sigma_\gamma^2}} \sigma_\gamma \end{cases}, \quad (11)$$

where R_{56} is the chicane strength, σ_{l0} the bunch length before the chicane. By calculating the bunch length and slice energy spread, one can now determine the slice emittance ε_{slice} and slice beam size $\sigma_{x-slice}$ at the center of the undulator can be expressed as:

$$\begin{cases} \sigma_{x-slice} = \sqrt{R_{11}^2 \sigma_{x0}^2 + R_{126}^2 \sigma_{x0}'^2 \sigma_{\gamma-slice}^2} \\ \varepsilon_{slice}^2 = \varepsilon_{x0}^2 + \frac{R_{126}^2}{R_{11}^2} \sigma_{x0}'^4 \sigma_{\gamma-slice}^2 \end{cases}, \quad (12)$$

4.2. Baseline Reference Case

At the start of COXINEL project, the baseline reference parameters that were examined at the source are presented in Table 3, where the electron beam is considered to be a round Gaussian beam. Our aim at COXINEL is to achieve FEL amplification at 200 nm. The line is optimized in such a way that $R_{11} = 10$ and $R_{56} = 0.4$ mm. Inserting these values in Equations (11) and (12), one gets the beam parameters at the center of the undulator as shown in Table 3.

Table 3. Baseline reference case parameters at the generation point in the gas jet and at the undulator center for $R_{56} = 0.4$ mm, $R_{11} = 10$ and $R_{126} = -4.4$.

Parameters	Symbol	Source	Undulator		Unit
			Total	Slice	
Energy	E	200	200	200	MeV
Normalized emittance	ε_N	1	2	1.13	π mm·mrad
Effective emittance	ε_{eff}	2.6	5	2.8	nm
Divergence (rms)	$\sigma_{x,z}'$	1	0.1	0.1	mrad
Beam size (rms)	$\sigma_{x,z}$	2.6	50	30	μ m
Bunch length (rms)	σ_l	1	4.3	-	μ m
Energy spread (rms)	$\sigma_{\gamma-slice}$	1	1	0.24	%
Total charge	Q	34	34	-	pC
Current	I_b	4.3	1	1	kA

4.3. Electron Beam Brightness

To qualify an electron beam for an FEL application, an important parameter, brightness, that combines emittance, current and energy spread, is examined. The electron beam brightness can be

defined in the 6D phase space \mathfrak{B}_{6D} as the total bunch charge Q divided by the normalized emittance in the three planes:

$$\mathfrak{B}_{6D} = \frac{Q}{\varepsilon_{nx}\varepsilon_{nz}\varepsilon_{ns}} = \frac{I}{\varepsilon_{nx}\varepsilon_{nz}\sigma_\gamma} \quad (13)$$

where $\varepsilon_{ns} = \sigma_s\sigma_\gamma$ scales as the product of bunch length and relative energy spread. At the generation source, the electron beam brightness is:

$$\mathfrak{B}_{6D} = 4.3 \times 10^5 \text{ A/mm}^2/\text{mrad}^2 \quad (14)$$

and at the center of the undulator:

$$\begin{cases} \mathfrak{B}_{6D}(\text{Total}) = 0.25 \times 10^5 \text{ A/mm}^2/\text{mrad}^2 \\ \mathfrak{B}_{6D}(\text{Slice}) = 3.3 \times 10^5 \text{ A/mm}^2/\text{mrad}^2 \end{cases} \quad (15)$$

Comparing the electron beam brightness generated with an LPA with the one using a conventional linac by taking typical values ($I_{peak} = 500 \text{ A}$, $\varepsilon_n = 1 \text{ mm}\cdot\text{mrad}$, $\sigma_\gamma = 0.01\%$), it is found to be $5 \times 10^6 \text{ A/mm}^2/\text{mrad}^2$, which is one order of magnitude higher due to the ultra-low energy spread.

As mentioned in the transport line description, an electron monochromator is placed in the middle of the chicane. This helps reduce the energy spread, decrease the emittance and increase the brightness at the center of the undulator [18,59].

5. Undulator Radiation Characteristics

As the electron wiggles inside the undulator, radiation is emitted at each period and adds constructively at the resonance wavelength λ and its harmonics:

$$\lambda = \frac{\lambda_u}{2n\gamma^2} \left[1 + \frac{K_u^2}{2} + \gamma^2\theta^2 \right] \quad (16)$$

with n the harmonic number and θ the observation angle.

5.1. Homogeneous Broadening

An electron orbiting an undulator with N_u periods produces a wavetrain with equal number of oscillations. The electric field E of the light wave is written as:

$$E(t) = \begin{cases} E_0 \exp(i\omega_1 t) & \text{if } -T/2 < t < T/2 \\ 0 & \text{Otherwise} \end{cases} \quad (17)$$

The time duration of the wave train is $T = N_u\lambda/c$, with c the speed of light. Due to its finite length, this wave train is not monochromatic but spans over a range of frequencies. This range can be determined by applying the Fourier transformation on the electric field:

$$E(\omega) = \frac{1}{\sqrt{2\pi}} \int_{-\infty}^{\infty} E(t)e^{-i\omega t} dt$$

$$E(\omega) = \frac{E_0}{\sqrt{2\pi}} \int_{-T/2}^{T/2} e^{i\Delta\omega t} dt \quad \text{with } \Delta\omega = \omega_1 - \omega.$$

Thus:

$$E(\omega) = \frac{2E_0}{\sqrt{2\pi}} \frac{\sin \Delta\omega T/2}{\Delta\omega}.$$

The spectral intensity ($I(\omega)$) is proportional to $|E(\omega)|^2$:

$$I(\omega) \propto \left(\frac{\sin x}{x}\right)^2, \quad (18)$$

with

$$x = \Delta\omega T/2 = \frac{(\omega_l - \omega)N_u\lambda}{2c} = \pi N_u \frac{\omega_l - \omega}{\omega_l}$$

The undulator homogeneous bandwidth is thus expressed as:

$$\left[\frac{\Delta\lambda}{\lambda}\right]_{hom} = \frac{\Delta\omega}{\omega} = \frac{1}{N_u}. \quad (19)$$

For the COXINEL undulator with 107 number of periods, the first harmonic natural line width is 0.93%.

5.2. Inhomogeneous Broadening

A real electron beam has a finite transverse emittance and a range in energy, which broadens the radiation bandwidth. The energy spread σ_γ widens the line symmetrically. By deriving Equation (16) with $\theta = 0$:

$$d\lambda = -\frac{\lambda}{2\gamma^2}(1 + K_u^2/2)\left(\frac{2d\gamma}{\gamma}\right).$$

Thus

$$\left[\frac{\Delta\lambda}{\lambda}\right]_{\sigma_\gamma} = 2\frac{d\gamma}{\gamma} = 2\sigma_\gamma. \quad (20)$$

For an energy spread of 0.2% rms, the contribution on the bandwidth is $\sim 0.94\%$ close to the natural linewidth of the 100 period undulator case.

The divergence $\sigma'_{x,z}$ causes a red shift of the resonant wavelength and widens the bandwidth asymmetrically.

$$\lambda = \frac{\lambda_u}{2\gamma^2}(1 + K_u^2/2) + \frac{\lambda_u}{2}\theta^2.$$

The deviation of the radiation wavelength with respect to the on-axis ($\theta = 0$):

$$\lambda - \lambda_{res} = \Delta\lambda = \lambda\gamma^2\theta^2/(1 + K_u^2/2).$$

Therefore

$$\left[\frac{\Delta\lambda}{\lambda}\right]_{\sigma'_{x,z}} = \frac{\gamma^2\sigma_{x,z}^2}{1 + K_u^2/2}. \quad (21)$$

A 0.1 mrad rms divergence contribution on the bandwidth is $\sim 0.1\%$ for an energy of 200 MeV and K_u of 2.

The total bandwidth can be calculated using the different contributions and applying an approximation that the divergence only contributes to the red side of the spectrum. Taking this into account, one can use the following quadratic sum approximation to determine the undulator radiation bandwidth [60]:

$$\left[\frac{\Delta\lambda}{\lambda}\right] = \frac{1}{2}\sqrt{\left[\frac{\Delta\lambda}{\lambda}\right]_{\sigma_\gamma}^2 + \left[\frac{\Delta\lambda}{\lambda}\right]_{hom}^2} + \sqrt{\frac{1}{4}\left[\frac{\Delta\lambda}{\lambda}\right]_{\sigma_\gamma}^2 + \frac{1}{4}\left[\frac{\Delta\lambda}{\lambda}\right]_{hom}^2 + \left[\frac{\Delta\lambda}{\lambda}\right]_{\sigma'_{x,z}}^2}. \quad (22)$$

Using Equation(22), the undulator radiation bandwidth is calculated using the total electron beam and slice parameters at the center of the undulator (see Table 3):

$$\begin{cases} \frac{\Delta\lambda}{\lambda}(Total) = 4.8\% \\ \frac{\Delta\lambda}{\lambda}(Slice) = 1.5\% \end{cases} \quad (23)$$

5.3. Photon Beam Flux and Brilliance

The photon flux \dot{N} at the first harmonic generated by an electron beam orbiting an undulator can be expressed as [61]:

$$\dot{N} = 1.43 \times 10^{14} \frac{N_u I K_u^2 |JJ|^2}{1 + K_u^2/2}. \quad (24)$$

The flux calculated in the case of COXINEL is 1.3×10^{19} ph/s/0.1% for a K_u value of 2. The flux is also simulated, for the total beam (blue) and slice beam (red) cases using an SRWcode [62] as shown in Figure 2. The flux is peaked at the resonant wavelength of 176 nm. The difference between the analytical value and the simulated one is due to the small aperture of the observation window. If one uses a larger aperture, the flux attains a value of 1.5×10^{19} ph/s/0.1% bw close to the calculated one. In addition, the relative bandwidth for the total beam and slice beam are found to be 4.9% and 1.4%, respectively, which are in good agreement with the calculated ones (see Equation (23)), implying that the approximation is quite valid.

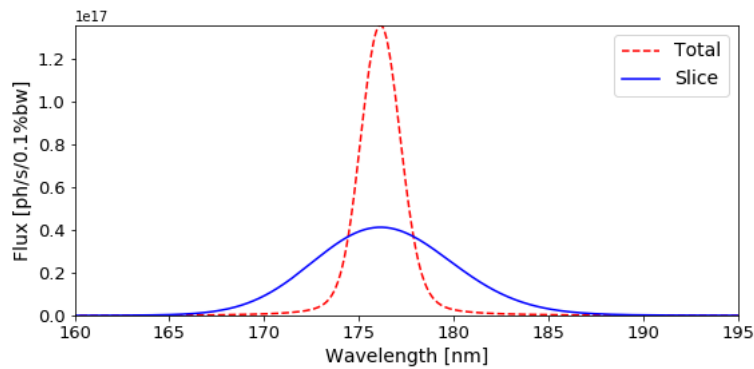


Figure 2. SRW simulations of the spectral flux using the beam parameters of Table 3 for the total beam (blue) and slice beam (red). Window aperture of 1 mm x 1 mm placed at a distance 10 m from the center of the undulator. $K_u = 2$.

The brilliance \mathfrak{B} refers to the number of photons with the same wavelength that are directed and concentrated on a spot per unit of time. \mathfrak{B} is expressed as the photon flux divided by the photon emittance:

$$\mathfrak{B} = \frac{\dot{N}}{4\pi^2 \Sigma_{x,z}^2 \Sigma'_{x,z} \frac{\Delta\lambda}{\lambda}}, \quad (25)$$

where

$$\begin{cases} \Sigma_{x,z} = \sqrt{\sigma_{x,z}^2 + \sigma_n^2} \\ \Sigma'_{x,z} = \sqrt{\sigma_{x,z}'^2 + \sigma_n'^2}, \end{cases} \quad (26)$$

with σ_n and σ_n' are the photon beam natural size and divergence, respectively and are expressed as [63–65]:

$$\begin{cases} \sigma_n = \sqrt{\frac{N_u \lambda_u \lambda}{4\pi}} \\ \sigma_n' = \sqrt{\frac{\lambda}{N_u \lambda_u}}. \end{cases} \quad (27)$$

The brilliance is calculated for the total electron beam and slice:

$$\begin{cases} \mathfrak{B}(Total) = 1.7 \times 10^{22} \text{ ph/s/mm}^2/\text{mrad}^2/0.1\%bw \\ \mathfrak{B}(Slice) = 7.5 \times 10^{22} \text{ ph/s/mm}^2/\text{mrad}^2/0.1\%bw. \end{cases} \quad (28)$$

The brilliance is also computed using SRW, where it is found to be 1.4×10^{22} ph/s/mm²/mrad²/0.1%bw for the total beam case and 7.6×10^{22} ph/s/mm²/mrad²/0.1%bw for the slice one. However, during the COXINEL experiment, the electron beam exhibited quite different qualities [66] and the brilliance is found to be of the orders of 10^{17} ph/s/mm²/mrad²/0.1%bw [53], 3 orders of magnitude lower than the calculated one.

6. FEL Evaluation

In this section, the Ming Xi equations [67], that allow for a quick evaluation of an FEL performance, are presented. The study is for SASE amplification where the lasing is achieved in a single pass of a high current, high brightness electron beam through a long undulator. Starting with the ideal case (1D model: electron beam has a uniform transverse spatial distribution with zero emittance and energy spread) as presented in Equation (8):

$$L_{1D} = \frac{\lambda}{4\pi\sqrt{3}\rho_{FEL}}. \quad (29)$$

It can be shown that the FEL gain length can be expressed by a universal scaling function:

$$\frac{L_{1D}}{L_g} = F(\eta_d, \eta_\epsilon, \eta_\gamma) = \frac{1}{1 + \eta}, \quad (30)$$

where

$$\eta_d = \frac{\lambda L_{1D}}{4\pi\sigma_x^2}, \quad \eta_\epsilon = \frac{4\pi\epsilon_n L_{1D}}{\gamma\beta\lambda}, \quad \eta_\gamma = \frac{4\pi\sigma_\gamma L_{1D}}{\lambda_u} \quad (31)$$

and

$$\eta = a_1\eta_d^{a_2} + a_3\eta_\epsilon^{a_4} + a_5\eta_\gamma^{a_6} + a_7\eta_\epsilon^{a_8}\eta_\gamma^{a_9} + a_{10}\eta_d^{a_{11}}\eta_\gamma^{a_{12}} + a_{13}\eta_d^{a_{14}}\eta_\epsilon^{a_{15}} + a_{16}\eta_d^{a_{17}}\eta_\epsilon^{a_{18}}\eta_\gamma^{a_{19}}, \quad (32)$$

with

$a_1 = 0.45$	$a_2 = 0.57$	$a_3 = 0.55$	$a_4 = 1.6$	$a_5 = 3$
$a_6 = 2$	$a_7 = 0.35$	$a_8 = 2.9$	$a_9 = 2.4$	$a_{10} = 51$
$a_{11} = 0.95$	$a_{12} = 3$	$a_{13} = 5.4$	$a_{14} = 0.7$	$a_{15} = 1.9$
$a_{16} = 1140$	$a_{17} = 2.2$	$a_{18} = 2.9$	$a_{19} = 3.2$	

The scaling parameters $\eta_d, \eta_\epsilon, \eta_\gamma$ measure the deviation of the beam from the ideal case, taking into account the gain reduction caused by diffraction, emittance and energy spread, respectively. The saturation power obtained from simulation is given by:

$$P_{sat} = 1.6\rho_{FEL} \left(\frac{L_{1D}}{L_g} \right) IE. \quad (33)$$

After the calculation of L_g and P_{sat} , the saturation length is determined by:

$$L_{sat} = L_g \ln \left(\frac{9P_{sat}}{P_n} \right), \quad (34)$$

where

$$P_n = c\rho_{FEL}^2 \frac{E}{\lambda},$$

where c is the speed of light. The power achieved after a certain undulator length can thus be determined using the following equation:

$$P = \frac{1}{9} P_n e^{s/L_g} \tag{35}$$

The calculated beam parameters presented in Table 3 are used to examine the FEL performance. Figure 3 shows the FEL power calculated as the chicane strength is varied for different magnification factors. The optimum case is for 0.2 mm chicane strength and 10 magnification factor, where the gain length is 0.11 m generating a power of 70 MW at 172 nm. The variation of the chicane strength provides an easy knob for FEL adjustment.

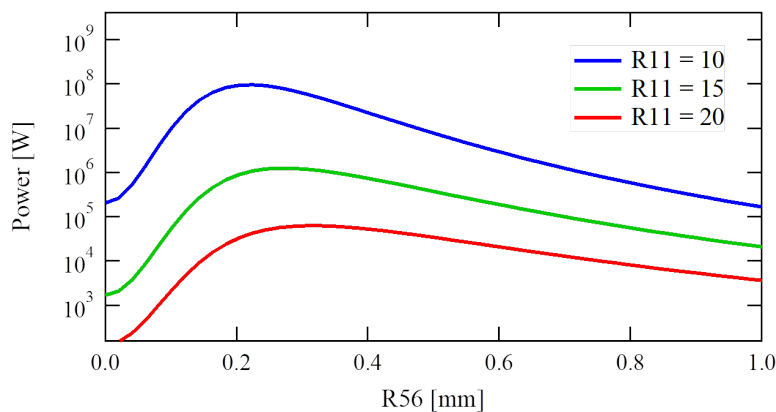


Figure 3. Free Electron Laser (FEL) power emitted after 2 m long undulator section as the magnification R_{11} and chicane strength R_{56} vary.

Table 4 presents the input values (R_{11} , R_{56}), the calculated beam parameters at the center of the undulator using Equation (12) and the FEL performance. The slice beam size and divergence highly depend on R_{11} whereas the slice energy spread depends only on R_{56} . The P_{COX} corresponds to the power that can be observed at COXINEL after the 2 m long undulator, where it reaches a maximum value of 70 MW for a magnification factor $R_{11} = 10$ and a chicane strength $R_{56} = 0.2$ mm.

Table 4. FEL performance as the magnification of the beam (source to undulator center) and chicane strength are varied. L_g the FEL gain length, L_{sat} the FEL saturation length, P_{sat} the saturation power.

Input		Beam Parameters						FEL Performance				
R_{11}	R_{126}	R_{56} mm	σ_L μm	σ_γ %	σ_x μm	σ'_x μrad	I_b kA	L_g m	P_{COX} MW	L_{sat} m	P_{sat} MW	
5	−9.1	0.4	4.3	0.24	25.6	200	1	0.14	3	2.8	978	
10	−4.5	0.4	4.3	0.24	28.2	100	1	0.12	17	2.5	1350	
15	−3	0.4	4.3	0.24	39.7	66.7	1	0.14	1	3.1	1188	
20	−2.3	0.4	4.3	0.24	52.3	50	1	0.17	0	3.7	1011	
30	−1.5	0.4	4.3	0.24	78.1	33.3	1	0.23	0	5	737	
10	0	0	1.6	1	26	100	2.8	0.17	0.2	3.5	1198	
10	−1.1	0.1	1.9	0.71	27.2	100	2.3	0.13	8	2.7	1938	
10	−2.3	0.2	2.5	0.45	27.9	100	1.7	0.11	70	2.4	2136	
10	−9.1	0.8	8.2	0.12	28.3	100	0.5	0.15	0.5	3	583	
10	−11.4	1	10.1	0.1	28.3	100	0.4	0.16	0.1	3.3	427	

7. Conclusions

The problems and the context of LPA based FEL have been reported. The state-of-art of LPA based undulator radiation is presented, where the radiation does not yet exhibit the same quality as those

achieved with conventional accelerators. FEL is still very challenging to achieve, using such a source, due to the large divergence and energy spread at the generation point. However, with a line designed to manipulate the electron beam phase space, such as COXINEL, FEL amplification is quite possible.

Author Contributions: Validation, A.G., O.M. and M.-E.C.; Formal analysis, A.G., D.O., S.C., M.L. and A.L.; Writing original draft preparation, A.G.; Writing—review and editing, A.G.; Supervision, M.-E.C.; Project administration, M.-E.C. All authors have read and agreed to the published version of the manuscript.

Funding: European Research Council for the Advanced Grants COXINEL (340015, PI: M.-E. Couprie), the EuPRAXIA design study (653782) and the Fondation de la Cooperation Scientifique (QUAPEVA-2012-058T), the Agence Nationale de la Recherche projet 239 Blanc DYNACO 2010-042301, and Ministry of Higher Education and Research.

Conflicts of Interest: The authors declare no conflict of interest.

References

1. Elder, F.; Gurewitsch, A.; Langmuir, R.; Pollock, H. Radiation from electrons in a synchrotron. *Phys. Rev.* **1947**, *71*, 829.
2. Madey, J.M. Stimulated emission of bremsstrahlung in a periodic magnetic field. *J. Appl. Phys.* **1971**, *42*, 1906–1913.
3. Colson, W. Theory of a free electron laser. *Phys. Lett. A* **1976**, *59*, 187–190.
4. Maine, P.; Strickland, D.; Bado, P.; Pessot, M.; Mourou, G. Generation of ultrahigh peak power pulses by chirped pulse amplification. *IEEE J. Quantum Electron.* **1988**, *24*, 398–403.
5. Tajima, T.; Dawson, J.M. Laser electron accelerator. *Phys. Rev. Lett.* **1979**, *43*, 267.
6. Malka, V.; Fritzler, S.; Lefebvre, E.; Aleonard, M.M.; Burgy, F.; Chambaret, J.P.; Chemin, J.F.; Krushelnick, K.; Malka, G.; Mangles, S.P.D.; et al. Electron Acceleration by a Wake Field Forced by an Intense Ultrashort Laser Pulse. *Science* **2002**, *298*, 1596–1600. doi:10.1126/science.1076782.
7. Esarey, E.; Schroeder, C.B.; Leemans, W.P. Physics of laser-driven plasma-based electron accelerators. *Rev. Mod. Phys.* **2009**, *81*, 1229–1285. doi:10.1103/RevModPhys.81.1229.
8. Malka, V. Laser plasma accelerators. *Phys. Plasmas* **2012**, *19*, 055501. doi:10.1063/1.3695389.
9. Schlenvoigt, H.P.; Haupt, K.; Debus, A.; Budde, F.; Jäckel, O.; Pfoth, S.; Schwoerer, H.; Rohwer, E.; Gallacher, J.; Brunetti, E.; et al. A compact synchrotron radiation source driven by a laser-plasma wakefield accelerator. *Nat. Phys.* **2008**, *4*, 130.
10. Fuchs, M.; Weingartner, R.; Popp, A.; Major, Z.; Becker, S.; Osterhoff, J.; Cortie, I.; Zeitler, B.; Hörlein, R.; Tsakiris, G.D.; et al. Laser-driven soft-X-ray undulator source. *Nat. Phys.* **2009**, *5*, 826.
11. Lambert, G.; Corde, S.; Phuoc, K.T.; Malka, V.; Ismail, A.B.; Benveniste, E.; Specka, A.; Labat, M.; Loulergue, A.; Briquez, F.; et al. Progress on the generation of undulator radiation in the UV from a plasma-based electron beam. In Proceedings of the 34th International Free-Electron Laser Conference, Nara, Japan, 26–31 August 2012.
12. Anania, M.P.; Brunetti, E.; Wiggins, S.; Grant, D.W.; Welsh, G.H.; Issac, R.; Cipiccia, S.; Shanks, R.; Manahan, G.; Aniculaesei, C.; et al. An ultrashort pulse ultra-violet radiation undulator source driven by a laser plasma wakefield accelerator. *Appl. Phys. Lett.* **2014**, *104*, 264102.
13. Grüner, F.; Becker, S.; Schramm, U.; Eichner, T.; Fuchs, M.; Weingartner, R.; Habs, D.; Meyer-ter Vehn, J.; Geissler, M.; Ferrario, M.; et al. Design considerations for table-top, laser-based VUV and X-ray free electron lasers. *Appl. Phys. B* **2007**, *86*, 431–435.
14. Pellegrini, C. Free electron lasers: Development and applications. *Part. Accel.* **1990**, *33*, 159–170.
15. Floettmann, K.; Paramonov, V.V. Beam dynamics in transverse deflecting rf structures. *Phys. Rev. Spec. Top.-Accel. Beams* **2014**, *17*, 024001.
16. Floettmann, K. Some basic features of the beam emittance. *Phys. Rev. Spec. Top.-Accel. Beams* **2003**, *6*, 034202.
17. Antici, P.; Bacci, A.; Benedetti, C.; Chiadroni, E.; Ferrario, M.; Rossi, A.; Lancia, L.; Migliorati, M.; Mostacci, A.; Palumbo, L.; et al. Laser-driven electron beamlines generated by coupling laser-plasma sources with conventional transport systems. *J. Appl. Phys.* **2012**, *112*, 044902.
18. Oumbarek Espinos, D.; Ghaith, A.; André, T.; Kitégi, C.; Sebdaoui, M.; Loulergue, A.; Marteau, F.; Blache, F.; Valléau, M.; Labat, M.; et al. Skew Quadrupole Effect of Laser Plasma Electron Beam Transport. *Appl. Sci.* **2019**, *9*, 2447.

19. Migliorati, M.; Bacci, A.; Benedetti, C.; Chiadroni, E.; Ferrario, M.; Mostacci, A.; Palumbo, L.; Rossi, A.; Serafini, L.; Antici, P. Intrinsic normalized emittance growth in laser-driven electron accelerators. *Phys. Rev. Spec. Top.-Accel. Beams* **2013**, *16*, 011302.
20. Huang, Z.; Kim, K.J. Three-dimensional analysis of harmonic generation in high-gain free-electron lasers. *Phys. Rev. E* **2000**, *62*, 7295.
21. Leemans, W.; Volfbeyn, P.; Guo, K.; Chattopadhyay, S.; Schroeder, C.; Shadwick, B.; Lee, P.; Wurtele, J.; Esarey, E. Laser-driven plasma-based accelerators: Wakefield excitation, channel guiding, and laser triggered particle injection. *Phys. Plasmas* **1998**, *5*, 1615–1623.
22. Lin, C.; van Tilborg, J.; Nakamura, K.; Gonsalves, A.J.; Matlis, N.H.; Sokollik, T.; Shiraishi, S.; Osterhoff, J.; Benedetti, C.; Schroeder, C.B.; et al. Long-range persistence of femtosecond modulations on laser-plasma-accelerated electron beams. *Phys. Rev. Lett.* **2012**, *108*, 094801.
23. Ghaith, A.; Oumbarek, D.; Kitégi, C.; Valléau, M.; Marteau, F.; Couprie, M.E. Permanent Magnet-Based Quadrupoles for Plasma Acceleration Sources. *Instruments* **2019**, *3*, 27.
24. Bennett, W.H. Magnetically self-focussing streams. *Phys. Rev.* **1934**, *45*, 890.
25. Rosenzweig, J.; Breizman, B.; Katsouleas, T.; Su, J. Acceleration and focusing of electrons in two-dimensional nonlinear plasma wake fields. *Phys. Rev. A* **1991**, *44*, R6189.
26. Chen, P. Grand disruption: A possible final focusing mechanism for linear colliders. *Part. Accel.* **1986**, *20*, 171–182.
27. Lehe, R.; Thaur, C.; Guillaume, E.; Lifschitz, A.; Malka, V. Laser-plasma lens for laser-wakefield accelerators. *Phys. Rev. Spec. Top.-Accel. Beams* **2014**, *17*, 121301.
28. Thaur, C.; Guillaume, E.; Döpp, A.; Lehe, R.; Lifschitz, A.; Phuoc, K.T.; Gautier, J.; Goddet, J.P.; Tafzi, A.; Flacco, A.; et al. Demonstration of relativistic electron beam focusing by a laser-plasma lens. *Nat. Commun.* **2015**, *6*, 6860.
29. Panofsky, W.K.H.; Baker, W.R. A focusing device for the external 350-MeV proton beam of the 184-inch cyclotron at Berkeley. *Rev. Sci. Instrum.* **1950**, *21*, 445–447.
30. Röckemann, J.H.; Schaper, L.; Barber, S.; Bobrova, N.; Boyle, G.; Bulanov, S.; Delbos, N.; Floettmann, K.; Kube, G.; Lauth, W.; et al. Direct measurement of focusing fields in active plasma lenses. *Phys. Rev. Accel. Beams* **2018**, *21*, 122801.
31. Tauschwitz, A.; Yu, S.; Eylon, S.; Bangerter, R.; Leemans, W.; Peters, C.; Rasmussen, J.; Reginato, L.; Barnard, J.; Sharp, W. Plasma lens focusing and plasma channel transport for heavy ion fusion. *Fusion Eng. Des.* **1996**, *32*, 493–502.
32. Nakanii, N.; Hosokai, T.; Iwasa, K.; Masuda, S.; Zhidkov, A.; Pathak, N.; Nakahara, H.; Mizuta, Y.; Takeguchi, N.; Kodama, R. Transient magnetized plasma as an optical element for high power laser pulses. *Phys. Rev. Spec. Top.-Accel. Beams* **2015**, *18*, 021303.
33. Van Tilborg, J.; Steinke, S.; Geddes, C.; Matlis, N.; Shaw, B.; Gonsalves, A.; Huijts, J.; Nakamura, K.; Daniels, J.; Schroeder, C.; et al. Active plasma lensing for relativistic laser-plasma-accelerated electron beams. *Phys. Rev. Lett.* **2015**, *115*, 184802.
34. Van Tilborg, J.; Barber, S.; Tsai, H.E.; Swanson, K.; Steinke, S.; Geddes, C.; Gonsalves, A.; Schroeder, C.; Esarey, E.; Bulanov, S.; et al. Nonuniform discharge currents in active plasma lenses. *Phys. Rev. Accel. Beams* **2017**, *20*, 032803.
35. Marochino, A.; Anania, M.; Bellaveglia, M.; Biagioni, A.; Bini, S.; Bisesto, F.; Brentegani, E.; Chiadroni, E.; Cianchi, A.; Croia, M.; et al. Experimental characterization of the effects induced by passive plasma lens on high brightness electron bunches. *Appl. Phys. Lett.* **2017**, *111*, 184101.
36. Pompili, R.; Anania, M.; Bellaveglia, M.; Biagioni, A.; Bini, S.; Bisesto, F.; Brentegani, E.; Cardelli, F.; Castorina, G.; Chiadroni, E.; et al. Focusing of High-Brightness Electron Beams with Active-Plasma Lenses. *Phys. Rev. Lett.* **2018**, *121*, 174801.
37. Seggebrock, T.; Maier, A.; Dornmair, I.; Grüner, F. Bunch decompression for laser-plasma driven free-electron laser demonstration schemes. *Phys. Rev. Spec. Top.-Accel. Beams* **2013**, *16*, 070703.
38. Maier, A.; Meseck, A.; Reiche, S.; Schroeder, C.; Seggebrock, T.; Gruener, F. Demonstration scheme for a laser-plasma-driven free-electron laser. *Phys. Rev. X* **2012**, *2*, 031019.
39. Loulergue, A.; Labat, M.; Evain, C.; Benabderrahmane, C.; Malka, V.; Couprie, M. Beam manipulation for compact laser wakefield accelerator based free-electron lasers. *New J. Phys.* **2015**, *17*, 023028.

40. Liu, T.; Zhang, T.; Wang, D.; Huang, Z. Compact beam transport system for free-electron lasers driven by a laser plasma accelerator. *Phys. Rev. Accel. Beams* **2017**, *20*, 020701.
41. Huang, Z.; Ding, Y.; Schroeder, C.B. Compact X-ray free-electron laser from a laser-plasma accelerator using a transverse-gradient undulator. *Phys. Rev. Lett.* **2012**, *109*, 204801.
42. Couprie, M.E.; Labat, M.; Evain, C.; Marteau, F.; Briquez, F.; Khojoyan, M.; Benabderrahmane, C.; Chapuis, L.; Hubert, N.; Bourassin-Bouchet, C.; et al. An application of laser plasma acceleration: towards a free-electron laser amplification. *Plasma Phys. Control. Fusion* **2016**, *58*, 034020.
43. André, T.; Szwaj, C.; Valléau, M.; Briquez, F.; Loulergue, A.; Hubert, N.; El Ajjouri, M.; Evain, C.; Goddet, J.P.; Rommeluère, P.; et al. Electron transport on Coxinel beam line. In Proceedings of the 8th International Particle Accelerator Conference (IPAC 2017), Copenhagen, Denmark, 14–19 May 2017.
44. Couprie, M.E.; André, T.; Andriyash, I. COXINEL: Towards free electron laser amplification to qualify laser plasma acceleration. *Reza Kenkyu* **2017**, *45*, 94–98.
45. Marteau, F.; Ghaith, A.; N’Gotta, P.; Benabderrahmane, C.; Valléau, M.; Kitegi, C.; Loulergue, A.; Vétéran, J.; Sebdaoui, M.; André, T.; et al. Variable high gradient permanent magnet quadrupole (QUAPEVA). *Appl. Phys. Lett.* **2017**, *111*, 253503.
46. Ghaith, A.; Kitegi, C.; André, T.; Valléau, M.; Marteau, F.; Vétéran, J.; Blache, F.; Benabderrahmane, C.; Cosson, O.; Forest, F.; et al. Tunable high gradient quadrupoles for a laser plasma acceleration based FEL. *Nucl. Instrum. Methods Phys. Res. Sec. A Accel. Spectrom. Detect. Assoc. Equip.* **2018**, *909*, 290–293.
47. Emma, P.; Bane, K.; Cornacchia, M.; Huang, Z.; Schlarb, H.; Stupakov, G.; Walz, D. Femtosecond and Subfemtosecond X-Ray Pulses from a Self-Amplified Spontaneous-Emission-Based Free-Electron Laser. *Phys. Rev. Lett.* **2004**, *92*, 074801. doi:10.1103/PhysRevLett.92.074801.
48. Scisciò, M.; Migliorati, M.; Palumbo, L.; Antici, P. Design and optimization of a compact laser-driven proton beamline. *Sci. Rep.* **2018**, *8*, 6299.
49. Zhu, X.; Broemmelsiek, D.R.; Shin, Y.M. Theoretical and numerical analyses of a slit-masked chicane for modulated bunch generation. *J. Instrum.* **2015**, *10*, P10042.
50. Benabderrahmane, C.; Valléau, M.; Ghaith, A.; Berteaud, P.; Chapuis, L.; Marteau, F.; Briquez, F.; Marcouillé, O.; Marlats, J.L.; Tavakoli, K.; et al. Development and operation of a Pr₂Fe₁₄B based cryogenic permanent magnet undulator for a high spatial resolution x-ray beam line. *Phys. Rev. Accel. Beams* **2017**, *20*, 033201.
51. Valléau, M.; Briquez, F.; Brunelle, P.; Kitegi, C.; Mary, A.; Rommeluère, P.; Béchu, N.; Somogyi, A.; Tilmont, M.; Idam, J.; et al. Construction and optimization of cryogenic undulators at SOLEIL. In Proceedings of the 60th ICFA Advanced Beam Dynamics Workshop on Future Light Sources (FLS2018), Shanghai, China, 5–9 March 2018.
52. Ghaith, A.; Somogyi, A.; Berteaud, P.; Couprie, M.E.; Valléau, M.; Sebdaoui, M.; Béchu, N.; Blache, F.; Briquez, F.; Tilmont, M.; et al. Progress of Pr₂Fe₁₄B based hybrid cryogenic undulators at SOLEIL. In Proceedings of the 8th International Particle Accelerator Conference (IPAC 2017), Copenhagen, Denmark, 14–19 May 2017.
53. Ghaith, A. Tunable High Spatio-Spectral Purity Undulator Radiation from a Transported Laser Plasma Accelerated Electron Beam. *Sci. Rep.* **2019**, *9*, 1–12.
54. Delbos, N.; Werle, C.; Dornmair, L.; Eichner, T.; Hübner, L.; Jalas, S.; Jolly, S.; Kirchen, M.; Leroux, V.; Messner, P.; et al. Lux—A laser–plasma driven undulator beamline. *Nucl. Instrum. Methods Phys. Res. Sec. A Accel. Spectrom. Detect. Assoc. Equip.* **2018**, *909*, 318–322.
55. Payet, J. Beta code. CEA, SACLAY. Available online: <http://irfu.cea.fr/Sacm/logiciels/index6.php> (accessed on 1 February 2017).
56. Khojoyan, M.; Briquez, F.; Labat, M.; Loulergue, A.; Marcouillé, O.; Marteau, F.; Sharma, G.; Couprie, M. Transport studies of LPA electron beam towards the FEL amplification at COXINEL. *Nucl. Instrum. Methods Phys. Res. Sec. A Accel. Spectrom. Detect. Assoc. Equip.* **2016**, *829*, 260–264.
57. Brown, K.L. *First-and Second-Order Matrix Theory for the Design of Beam Transport Systems and Charged Particle Spectrometers*; Technical Report; Stanford Linear Accelerator Center: Menlo Park, CA, USA, 1971.
58. Thomas, A. Transport et Manipulation D’élECTrons Produits par Interaction Laser Plasma sur la Ligne COXINEL. Ph.D. Thesis, Paris Saclay, Essonne, France, 2018.
59. Oumbarek, D. COXINEL transport of laser plasma accelerated electrons. accepted.
60. Ghaith, A. Towards Compact and Advanced Free Electron Laser. Ph.D. Thesis, Paris Saclay, Essonne, France, 2019.

61. Clarke, J.A. *The Science and Technology of Undulators and Wigglers*; Oxford University Press: Oxford, UK, 2004; Volume 4,
62. Chubar, O.; Elleaume, P.; Kuznetsov, S.; Snigirev, A.A. Physical optics computer code optimized for synchrotron radiation. *Opt. Des. Anal. Softw. II Int. Soc. Opt. Photon.* **2002**, 4769, 145–152.
63. Coisson, R.; Walker, R. Phase space distribution of brilliance of undulator sources. Insertion Devices for Synchrotron Sources. *Int. Soc. Opt. Photonics* **1986**, 582, 24–31.
64. Kim, K.-J. Brightness and Coherence of Radiation from Undulators and High-Gain Free Electron Lasers. *Nucl. Instrum. Methods Phys. Res. Sec. A Accel. Spectrom. Detect. Assoc. Equip.* **1987**, 261, 44–53.
65. Walker, R.P. Insertion Devices: Undulators and Wigglers. In Proceedings of the CERN Accelerator School: Course on Synchrotron Radiation and Free-electron Lasers, Grenoble, France, 22–27 April 1996; pp. 129–190.
66. André, T.; Andriyash, I.; Loulergue, A.; Labat, M.; Roussel, E.; Ghaith, A.; Khojoyan, M.; Thaury, C.; Valléau, M.; Briquez, F.; et al. Control of laser plasma accelerated electrons for light sources. *Nat. Commun.* **2018**, 9, 1334.
67. Xie, M. Design optimization for an X-ray free electron laser driven by SLAC linac. In Proceedings of the Particle Accelerator Conference, Dallas, TX, USA, 1–5 May 1995; Volume 1, pp. 183–185.



© 2020 by the authors. Licensee MDPI, Basel, Switzerland. This article is an open access article distributed under the terms and conditions of the Creative Commons Attribution (CC BY) license (<http://creativecommons.org/licenses/by/4.0/>).